Neuron, Vol. 46, 333–346, April 21, 2005, Copyright ©2005 by Elsevier Inc. DOI 10.1016/j.neuron.2005.03.002

Does Neuronal Synchrony Underlie Visual Feature Grouping?

Ben J.A. Palanca and Gregory C. DeAngelis*
Department of Anatomy and Neurobiology
Washington University School of Medicine
Box 8108
660 South Euclid Avenue
Saint Louis, Missouri 63110

Summary

Previous research suggests that synchronous neural activity underlies perceptual grouping of visual image features. The generality of this mechanism is unclear, however, as previous studies have focused on pairs of neurons with overlapping or collinear receptive fields. By sampling more broadly and employing stimuli that contain partially occluded objects, we have conducted a more incisive test of the binding by synchrony hypothesis in area MT. We find that synchrony in spiking activity shows little dependence on feature grouping, whereas gamma band synchrony in field potentials can be significantly stronger when features are grouped. However, these changes in gamma band synchrony are small relative to the variability of synchrony across recording sites and do not provide a robust population signal for feature grouping. Moreover, these effects are reduced when stimulus differences nearby the receptive fields are eliminated using partial occlusion. Our findings suggest that synchrony does not constitute a general mechanism of visual feature binding.

Introduction

The visual system rapidly groups diverse image features into coherent representations of objects, but the neural mechanisms underlying this process are poorly understood. Because different parts of an object are often represented by neurons that are distributed across cortical areas, these distant neural signals must be somehow combined to form a representation of the object. This is referred to as the *binding problem* (Treisman, 1996; von der Malsburg, 1995; Wolfe and Cave, 1999). How the binding problem might be solved by the visual system has been a matter of intense debate (Ghose and Maunsell, 1999; Golledge et al., 1996; Gray, 1999; Riesenhuber and Poggio, 1999; Shadlen and Movshon, 1999; Singer, 1999).

One proposed solution to the binding problem is that synchronous neural activity provides a temporal code for grouping together parts of an object (Eckhorn et al., 1988; Gray, 1999; Gray et al., 1989; Singer and Gray, 1995; von der Malsburg and Schneider, 1986). According to this binding by synchrony (BBS) hypothesis, "spatially segregated neurons should exhibit synchronized response episodes if activated by a single stimulus or by stimuli that can be grouped together into a single perceptual object" (Singer, 1997). Numerous studies have examined this hypothesis experimentally (Brosch et al., 1997; Castelo-Branco et al., 2000; Engel et al., 1991a; Freiwald et al., 1995; Fries et al., 1997; Gail et al., 2000; Golledge et al., 2003; Gray et al., 1989; Kreiter and Singer, 1996; Lamme and Spekreijse, 1998; Livingstone, 1996; Thiele and Stoner, 2003; Woelbern et al., 2002), but the evidence remains controversial and incomplete.

A common experimental paradigm used to test the BBS hypothesis involves measuring the responses of two groups of neurons to either a pair of optimally oriented stimuli (bars or gratings) or a single stimulus having properties intermediate between the preferences of the two groups (Castelo-Branco et al., 2000; Engel et al., 1991a; Engel et al., 1991b; Gray et al., 1989; Kreiter and Singer, 1996; Livingstone, 1996). These studies find that synchrony is generally stronger for the single stimulus. The most striking of these results was reported by Kreiter and Singer (1996). Multiunit (MU) recordings were taken from pairs of sites in the middle temporal (MT) area with overlapping receptive fields (RFs), and these were stimulated with either a pair of optimally directed moving bars or a single, intermediate moving bar. In every experiment, Kreiter and Singer (1996) found stronger synchrony for the single bar stimulus, consistent with the BBS hypothesis. We took this strong effect as a starting point for our investigations.

Our experiments address three limitations of previous studies. First, in comparing "bound" versus "unbound" stimulus conditions, previous studies have generally relied on pairs of stimuli that differed within, or immediately around, the classical RFs of the recorded neurons. These stimuli elicit different temporal patterns of activation, including differential activation of common inputs, thus complicating the analysis and interpretation of synchrony. To provide a more incisive test of the BBS hypothesis, we compare conditions in which stimuli within the classical RFs of the two recording sites are identical. Moreover, using displays that depict partially occluded objects, we are able to compare bound versus unbound conditions in which stimulus differences are confined to regions outside the classical RFs. Second, previous studies have focused on pairs of neurons with either overlapping RFs or nonoverlapping but collinear RFs (collinear RFs have their centers aligned parallel to a common orientation preference). It is known that there are dense interconnections among neurons with overlapping RFs (Gilbert and Wiesel, 1979; Gilbert and Wiesel, 1983; Kisvarday et al., 1993; Kisvarday et al., 1997; Rockland and Lund, 1983), as well as extensive horizontal connections among neurons with similar orientation preferences (Gilbert and Wiesel, 1989; Ts'o et al., 1986). Thus, synchrony among these neurons could be an epiphenomenon of cortical wiring, rather than a neural basis for feature binding per se (Lamme and Spekreijse, 1998). The BBS hypothesis, in its most general form (Singer, 1997), predicts that synchrony should correlate with feature grouping even among neurons with nonoverlapping, noncollinear RFs.

*Correspondence: gregd@cabernet.wustl.edu

We have mainly focused our experiments on such pairs of neurons, as they have not been studied systematically with stimuli that differ only outside the classical RF. Third, previous studies have not examined whether stimulus-related differences in synchrony strength are large enough, relative to variations in synchrony across recording sites, to be useful for perceptual feature grouping. Our analyses address this issue more directly, through the use of an ideal observer model.

We examined synchrony in area MT using both MU recordings and local field potentials (LFPs), as these have been purported to be more sensitive measures of synchrony than single-unit recordings (Bedenbaugh and Gerstein, 1997; Brosch et al., 1997; Frien et al., 1994). LFPs reflect synchrony over greater cortical distances, making them well suited to the study of nonoverlapping RFs (Engel et al., 1990; Frien and Eckhorn, 2000; Gail et al., 2000). Our findings from MT cast doubt on the notion that synchrony provides a general mechanism for linking visual features that are grouped perceptually.

Results

We measured MU activity and LFPs from paired electrode recordings in area MT of two fixating macaque monkeys. Before examining how neuronal synchrony varied with the grouping of features into objects, we first measured the direction tuning and quantitatively mapped the RF at each recording site based on MU activity (see Experimental Procedures).

Experiment 1: Effect of Figure Grouping on Neuronal Synchrony

Our primary goal was to determine whether synchrony between pairs of recording sites with nonoverlapping RFs depends on the grouping of image features into one versus two objects. The visual stimuli were tailored to match the preferences of the two MT recording sites, while minimizing stimulus differences within the classical MU RFs (see Experimental Procedures). Stimulus differences promoting feature grouping were thus restricted to the nonclassical RF surround, when present (Allman et al., 1985). Figure 1 shows data from an example experiment. In one condition (Figure 1A), the two nonoverlapping RFs were stimulated with a single closed figure; in the other condition (Figure 1B), the two RFs were stimulated with two separate closed figures. All stimulus conditions were randomly interleaved within a single block of trials. As shown in the peristimulus time histograms (PSTHs) of MU responses (Figures 1C and 1D), the firing rates were modulated by the periodic 1 Hz motion of the figures through the RFs. Note that the two PSTHs are virtually identical, because motions of the line segments within the classical RFs were matched under the two conditions. Indeed, across 112 data sets, we found no significant difference in mean firing rates ($p = 0.18$, Scheffe's post hoc test) (see Figure S1, leftmost column, in the Supplemental Data available with this article online).

We quantified the strength of synchrony in LFP and MU responses by computing coherency spectrograms using multitaper spectral analysis (see Experimental Procedures). This method provides a single framework for analyzing correlations in both continuous signals (LFPs) and point processes (MU) (Halliday and Rosenberg, 1999; Mitra and Pesaran, 1999). It also allowed us to distinguish correlations in the γ frequency band (30–80 Hz) from those in lower frequencies (0–30 Hz). The magnitude of the coherency, |Coherency|, is plotted as a function of time (0–3000 ms) and frequency (0–100 Hz) and provides a measure of the correlation between neural signals in each frequency band at each point in time during stimulus presentation. Figures 1E and 1F show |Coherency| spectrograms for LFP signals from the example experiment described above. To simplify these data, we collapse each spectrogram into a single curve by computing |Coherency| over the time epochs that elicited significant MU responses from both recording sites (dashed vertical lines in Figures 1C and 1D; see Experimental Procedures). The resulting |Coherency| spectra are shown in Figure 1G (red curve for the single object condition). LFP |Coherency| is strongest at low frequencies, as reported elsewhere (Gail et al., 2000; Pesaran et al., 2002), but substantial power is also seen in the gamma band (30–80 Hz). In this experiment, there is slightly stronger synchrony in the gamma band for one figure versus two figures, but the effect is small.

Similar data were obtained from 112 pairs of recording sites for which the two MT RFs were stimulated with a single closed figure, two separate closed figures, or two isolated bars. In roughly half of the data sets, the two separate figures (or bars) shared a common movement trajectory as shown in Figures 1A and 1B. In the remaining cases, different global motion trajectories were given to the two figures, such that there was relative motion between them. Since no significant difference was found between these two subsets of data, we pooled them for analysis (see Figure S2). From the coherency spectra, average |Coherency| was computed in two frequency bands: 0–30 Hz and 30–80 Hz (gamma band).

Figure 2A shows population LFP data for the comparison between a single closed figure and two separate closed figures. Filled and open data points denote the two frequency bands of interest, whereas circles and triangles indicate data from two different monkeys. Across the population, the single figure elicited significantly stronger synchrony than the two separate figures in both the 0–30 Hz band ($p < 0.001$, Scheffe's test) and the 30–80 Hz band ($p = 0.01$, Scheffe's test). Note, however, that these differences are quite small relative to the range of |Coherency| values observed across experiments, a point to which we shall return later.

Figure 2B shows analogous data obtained from analyzing MU responses at the same 112 pairs of recording sites. These data differ from the LFP data in two respects. First, |Coherency| values from MU responses are an order of magnitude smaller than those from LFP signals, indicating that MU synchrony was generally very weak for pairs of sites with nonoverlapping RFs. Second, we find no significant difference in MU synchrony between the one figure and two figures conditions for the 30–80 Hz band ($p = 0.83$, Scheffe's test), and only a marginally significant difference for the 0–30 Hz band ($p = 0.04$, Scheffe's test). Thus, stimulus-related differences in synchrony were less pronounced in MU responses than in LFPs.

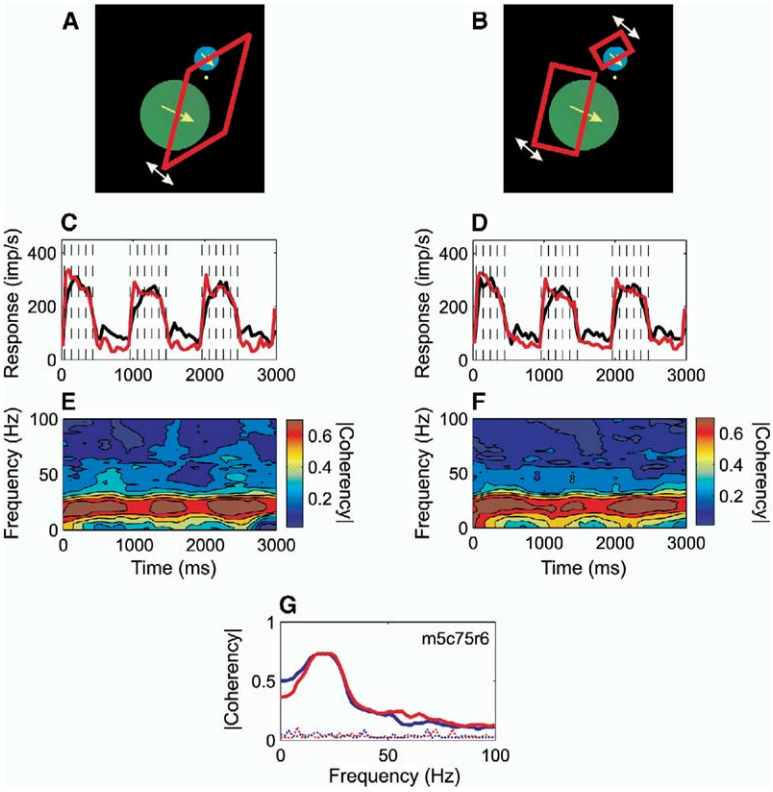

Figure 1. Experiment 1: Dependence of Neuronal Synchrony on Feature Grouping for One Pair of Recording Sites in Visual Area MT

(A) Stimulus configuration for the one figure condition. Colored circles indicate the receptive field (RF) boundaries for a pair of recording sites, and arrows denote the preferred directions of motion. Here, both RFs were stimulated with a single moving polygon.

(B) Stimulus configuration for the two figures condition. The two RFs are stimulated with separate polygons, but motion within the classical RFs is identical to that in (A).

(C) PSTHs of MU activity in response to the one figure condition. Red and black traces show responses of the two recording sites. Dashed vertical lines show 100 ms time epochs in which both groups of neurons were significantly active.

(D) PSTHs of MU responses for the two figures condition.

(E) |Coherency| spectrogram computed from LFPs recorded in the one figure condition. |Coherency| (color coded) is plotted against time and frequency.

(F) |Coherency| spectrogram for the two figures condition.

(G) Simplified |Coherency| functions obtained by averaging coherency across all 100 ms time epochs containing significant MU responses (dashed vertical lines in [C] and [D]). Red curve: one figure condition. Blue curve: two figures condition. Dashed curves show |Coherency| functions computed from shuffled trials, indicating the levels of coherency expected by chance.

The BBS hypothesis also predicts that synchrony should be stronger for a single closed figure than for two isolated bars (see insets to Figure 2C). Consistent with this prediction, we observed significantly larger LFP |Coherency| in the 30–80 Hz band for one figure versus two bars (open symbols, Figure 2C; $p < 0.001$, Scheffe's test), although the effect was again quite small. Surprisingly, however, we found the opposite effect (stronger LFP synchrony for two bars than one figure) in the 0–30 Hz band (filled symbols, Figure 2C; $p < 0.001$, Scheffe's test). Thus, the strength of LFP synchrony in the 0–30 Hz band is clearly stimulus dependent, but the relevant aspect of the stimuli that modulates synchrony is not whether the features are grouped into one object versus two objects. Figure 2D shows the analogous data obtained from MU responses. In this case, there is no significant difference in |Coherency| between one figure and two bars in either the 0–30 Hz band ($p = 0.24$, Scheffe's test) or the 30–80 Hz band ($p = 0.59$, Scheffe's test).

Overall, the data of Figure 2 provide limited support for the BBS hypothesis. Gamma band LFP synchrony is weakly consistent with BBS predictions, but low-frequency LFP synchrony and MU synchrony do not vary as expected from the BBS hypothesis.

Experiment 2: Neural Correlates of Feature Grouping across Occluders

The data of Figure 2 suggest that synchrony depends on stimulus differences outside of the classical RF, but not necessarily on feature grouping per se. In an effort to dissociate feature grouping from local stimulus context, we made use of stimuli that depict the global motion of a partially occluded object. In these stimuli, a parallelogram translates along a linear or circular trajectory, and the figure is viewed through a set of four apertures such that the corners of the moving object are never visible. The apertures were either visible (Figure 3A, top left inset) or invisible (Figure 3A, bottom-right inset) depending on the relative luminance of the background and apertures. Human psychophysical studies have shown that naive subjects correctly perceive the global motion direction of the figure when apertures are visible, but not when they are invisible (Lorenceau and Shiffrar, 1992). Thus, the BBS hypothesis predicts stronger synchrony for visible apertures.

Figure 3A shows the result of this comparison for LFP |Coherency| (same format as Figure 2). Across 96 experiments, gamma band LFP synchrony is slightly, but significantly ($p < 0.001$, Scheffe's test), stronger for visible apertures than invisible apertures. In contrast, there is no significant difference for 0–30 Hz LFP synchrony ($p = 0.21$, Scheffe's test). Figure 3B shows the analogous results for MU coherency. In this case, synchrony is significantly stronger for visible apertures in the 0–30 Hz band ($p < 0.001$, Scheffe's test), but not in the 30–80 Hz band ($p = 0.51$, Scheffe's test).

These results appear to support the BBS hypothesis. However, we also included a control condition in which a mask with visible apertures was presented alone, without moving stimuli in the classical RFs. Surprisingly, the static apertures alone produced much stronger syn-

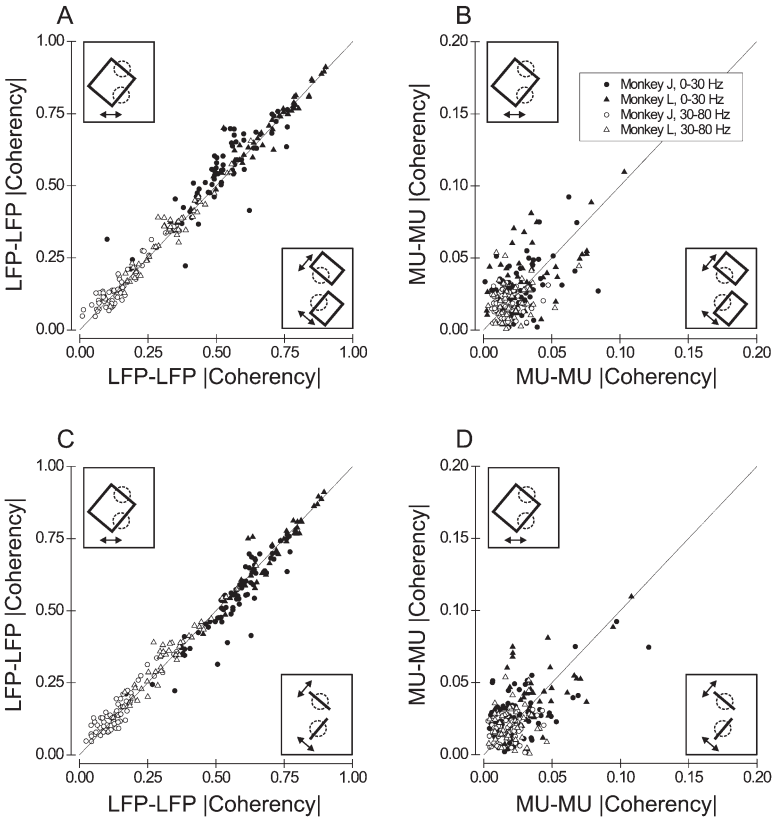

Figure 2. Population Data for Experiment 1

(A) The magnitude of LFP coherency for the one figure condition is plotted against that for the two figures condition. Filled and open symbols denote the 0–30 Hz and 30–80 Hz frequency bands, respectively. Circles and triangles denote data from monkeys J and L, respectively (n = 112 pairs total). The diagonal line has unity slope. The BBS hypothesis predicts that data points should lie above the diagonal.

(B) Same as (A), except that data are shown for MU |Coherency| measurements.

(C) LFP |Coherency| for the one figure condition is plotted against LFP coherency for the two bars condition.

(D) Same as (C), except that data are shown from MU |Coherency| measurements.

chrony than the moving bars inside invisible apertures (Figures 3C and 3D). This effect was highly significant in both frequency bands for LFP |Coherency|, and in the 0–30 Hz band for MU responses ($p < 0.001$, Scheffe's test). The apertures alone also produced significantly stronger synchrony than the moving figure behind visible apertures (data not shown; $p < 0.001$).

Our findings indicate that the stronger synchrony observed with visible versus invisible apertures (Figures 3A and 3B) is due to the mere presence of static apertures along the fringes of the classical RFs and is not necessarily a neural correlate of feature grouping per se. Consistent with the low-frequency coherency data from experiment 1 (Figures 2A and 2C), this shows that synchrony can depend on stimulus configuration in unexpected ways that may not reflect feature grouping.

Experiment 3: Temporal History and Feature Grouping across Occluders

In experiment 2, the effect of static apertures on synchrony strength was an unexpected confound, given that moving features in the RFs were identical for both visible and invisible apertures. To remove this confound, we performed an additional experiment using an extended mask that again contained two apertures positioned over the classical RFs of the two recording sites (Figure 4A). Visual stimuli—either a single angle figure or two separate bars—initially appeared to one side of the mask and then moved behind the mask such that portions of the figures stimulated the two RFs. Importantly, once the stimuli passed behind the mask, visual stimulation within and immediately around the RFs was identical regardless of whether one figure or two bars appeared to be moving behind the mask. No corners or line endings were visible outside the mask while bars were present within the RFs. Thus, only the temporal history of stimulation outside of the mask determined whether the two bars appeared to be connected. As an interleaved control, we also presented the identical moving visual stimuli without the occluding mask (Figure 4B).

This experiment was performed at 45 pairs of recording sites with nonoverlapping RFs. When the occluding mask was absent (as depicted in Figure 4B), we found significantly stronger LFP synchrony in the 30–80 Hz band for the single angle figure than for the two separate bars ($p = 0.02$, Scheffe's test; data not shown). LFP synchrony in the 0–30 Hz band did not differ between the two visual stimuli ($p = 0.63$, Scheffe's test). Thus, in the absence of the mask, our findings were largely consistent with those of Figures 2C and 2D.

Figure 4C shows data from interleaved trials in which the mask was present over the two RFs (e.g., Figure 4A). In this case, we find no significant difference in LFP synchrony between one figure and two bars for both the 0–30 Hz band ($p = 0.68$, Scheffe's test) and the 30–80 Hz band ($p = 0.64$, Scheffe's test). Similar results were obtained for synchrony measurements derived from MU activity recorded at the same 45 pairs of recording sites (Figure 4D) ($p > 0.3$ for both frequency bands). Thus, the data of Figure 4 show that synchrony did not vary with feature grouping when stimulus differ-

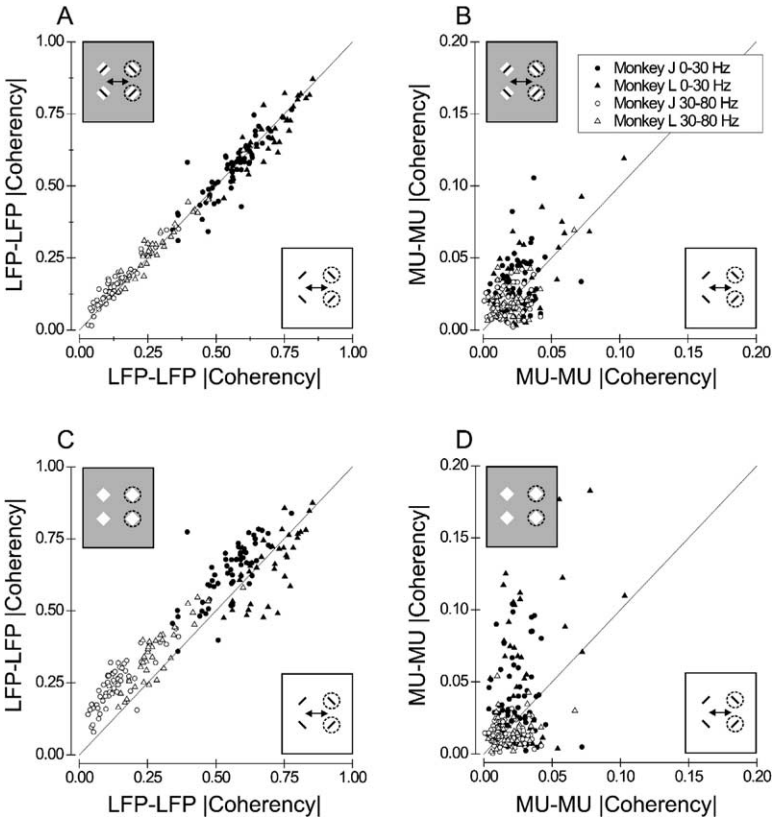

Figure 3. Results from Experiment 2

(A) Comparison of LFP |Coherency| between stimulus conditions with visible apertures (ordinate) and invisible apertures (abscissa). In each case, a moving parallelogram was partially occluded such that the corners were never visible. Data are shown for 96 pairs of recording sites.

(B) Comparison of MU |Coherency| between the visible and invisible aperture conditions.

(C) LFP |Coherency| measured in response to the static visible apertures alone (no moving figure) is plotted as a function of |Coherency| for the invisible aperture condition (with figure motion).

(D) MU |Coherency| for the static apertures alone versus the invisible aperture condition.

ences within and immediately around the classical RFs were eliminated with the use of an occluding mask.

Experiment 4: Synchrony among Neurons with Overlapping RFs

Since our experiments involving nonoverlapping RFs provided little support for the BBS hypothesis, we sought to replicate the findings of Kreiter and Singer (1996) in which stronger synchrony was observed for one moving bar versus two moving bars. Thus, we recorded from pairs of locations in MT that had overlapping RFs (average overlap of 38%, as compared to 5% for experiments 1–3), and we presented either a pair of optimally directed bars or a single bar of intermediate direction (see insets to Figure 5A).

Figure 5A summarizes results from LFP measurements at 99 pairs of recording sites in MT. Significantly stronger synchrony was observed when neurons were activated by a single bar than by two separate bars, and this was true for both frequency bands of interest ($p < 10^{-5}$, Scheffe's test). However, the effect was again quite small relative to the variation in |Coherency| across the population. Figure 5B shows analogous results for MU activity from 128 pairs of recording sites. No significant difference in synchrony between one bar and two bars was found in the 0–30 Hz band ($p = 0.32$, Scheffe's test), but significantly stronger synchrony was observed for one bar versus two bars in the 30–80 Hz band ($p < 10^{-5}$, Scheffe's test). While the latter result is consistent with Kreiter and Singer's analysis of MU responses in MT, the magnitude of the effect in our data set is much smaller (compare to their Figure 2A).

Our findings might differ from those of Kreiter and Singer (1996) because we assessed synchrony using spectral coherency analysis, whereas they used conventional cross-correlation analysis. Thus, we computed cross-correlograms of MU responses and quantified synchrony using two metrics: the r_{CCG} metric of Bair et al. (2001) (see Experimental Procedures) and the NC metric used by Kreiter and Singer (1996). Figure 5C shows r_{CCG} values obtained from 128 pairs of recording sites during the one bar versus two bars experiment. Pairs for which statistically significant (bootstrap test, $p < 0.05$) synchrony was observed under either stimulus condition are shown by filled symbols. Using the r_{CCG} metric, we found significantly stronger synchrony for one bar versus two bars across the population ($p = 0.01$, Scheffe's test), but again the magnitude of the effect was much smaller than that seen by Kreiter and Singer. Our results using the r_{CCG} metric were instead quite comparable to those found using coherency analysis in the 0–30 Hz band (Figure 5B).

We also quantified our results using the NC metric of Kreiter and Singer, which is derived by fitting modified Gabor functions to raw cross-correlograms (Konig, 1994). Figure 5D summarizes the results of the one bar versus two bars experiment using the NC metric. Here again, we find significantly stronger synchrony for one bar versus two bars ($p < 0.001$, Scheffe's test), but the effect is much weaker than that reported by Kreiter and Singer, who found a larger NC value for the one bar

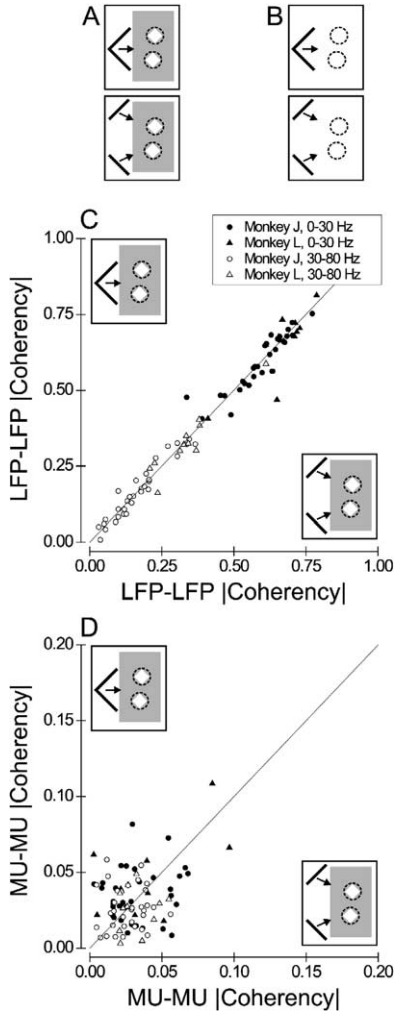

Figure 4. Results from Experiment 3

(A) An opaque mask (gray rectangle) containing two apertures was placed over the RFs (dashed circles) of a pair of MT recording sites. Either a single angle contour (top) or a pair of separate bars (bottom) was passed behind the occluding mask to stimulate the two RFs.

(B) These two stimulus conditions were identical to those in (A), except that the occluding mask was not present.

(C) The magnitude of LFP coherency in the occluded angle condition is plotted against that for the occluded bars (n = 45 pairs of recording sites).

(D) Same as (C), except that MU |Coherency| data are shown.

condition in 26/26 experiments. In contrast, only half of our 128 data sets had nonzero NC values for both stimulus conditions; among these, one-third showed larger NC values for two bars. Overall, it does not appear that the method by which synchrony is assessed can account for the differences between our results and those of Kreiter and Singer (see Discussion).

It should also be noted that pairs of recording sites that have statistically significant r_{CCG} values (filled symbols in Figure 5C) frequently have very small NC values (filled symbols in Figure 5D), whereas pairs of sites with nonsignificant r_{CCG} values frequently have large NC values. Overall, there is only a marginally significant correlation (Spearman r = 0.19; $p < 0.03$) between r_{CCG} and NC values across our sample of 128 MU recordings.

Population Summary

Figure 6 summarizes the relationships between synchrony and feature grouping across our four sets of experiments. The average difference in synchrony strength between one object and two objects is shown for each different stimulus configuration (iconized in Figure 6A), along with 95% confidence intervals around the mean. Data from LFP coherency analysis (Figure 6B), MU coherency analysis (Figure 6C), and conventional MU cross-correlation analysis (Figure 6D) are shown separately. The BBS hypothesis predicts that differences in synchrony strength should be significantly larger than zero for all stimulus comparisons. The statistical significance of each datum (relative to zero) was assessed using a general linear model (GLM) that included terms to account for differences in RF overlap, differences in preferred direction, and differences between monkeys. Most of the significant differences in synchrony were found among LFP recordings, particularly in the 30–80 Hz gamma band. In contrast, LFP synchrony in the 0–30 Hz band was not a reliable indicator of feature grouping. Synchrony in MU responses generally did not show any strong dependency on feature grouping, with two notable exceptions being the one bar versus two bars condition from experiment 4 and the invisible apertures versus "mask only" condition from experiment 2. Importantly, when stimulus differences within and immediately around the RFs were eliminated using occluders (sixth column in Figure 6; experiment 3), none of the synchrony metrics showed a significant dependence on feature grouping.

Differences in synchrony strength between stimulus conditions are more difficult to interpret when there are corresponding changes in mean firing rates, due to the general ambiguity in attributing weaker correlations to fewer correlated spikes versus greater uncorrelated spikes. Except for experiment 4 (and the mask only condition of experiment 2), our stimuli were constructed to minimize differences in firing rates between one object and two object conditions. Figure S1 confirms that, overall, there were no significant differences in mean firing rates between one object and two object conditions for experiments in which stimuli were held constant within the classical RFs (columns 1, 2, 3, 5, and 6 of Figure S1). In contrast, the two bar condition of experiment 4 elicited significantly stronger responses than the one bar condition, as expected since the two bars matched the preferred directions of each pair of recording sites.

Dependence of Synchrony on RF Parameters versus Feature Grouping

A wide variance in synchrony strength was observed across recording sites within each experiment, particularly among LFP recordings (see Figures 2–5). In contrast to the weak effects of feature grouping on synchrony that are summarized in Figure 6, we found strong dependencies of synchrony on RF overlap and difference in preferred directions. Using these two basic RF parameters and monkey identity as independent

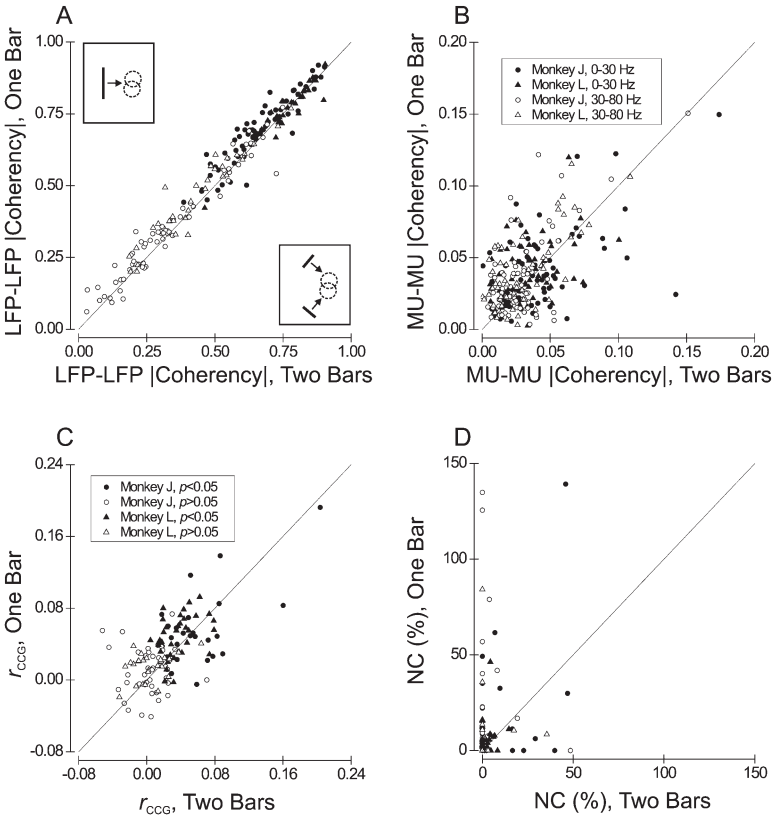

Figure 5. Results from Experiment 4, in which a Pair of Overlapping RFs Was Stimulated with a Pair of Optimally Directed Bars or a Single Bar of Intermediate Direction

In each graph, synchrony strength in response to the single bar is plotted on the ordinate, and synchrony for the two separate bars is plotted on the abscissa. (A) LFP coherency data from 99 pairs of recording sites. (B) MU coherency data from 128 pairs of recording sites. (C) Normalized cross-correlogram area (r_{CCG}) for the one bar condition is plotted against that for the two bar condition (n = 128). Filled symbols indicate values of r_{CCG} that are significantly greater than zero ($p < 0.05$, permutation test). (D) The NC metric of synchrony strength (Kreiter and Singer, 1996) is plotted in the same format as (C) (n = 128). Filled symbols again represent significant synchrony based on the corresponding r_{CCG} metric.

variables in the GLM described above, we found that all measures of synchrony strength were positively correlated with RF overlap, and negatively correlated with the difference in preferred directions between members of a pair of recording sites (Table 1). With this GLM, we were able to account for 6%–52% of the total variance in synchrony strength, as shown in Table 2 (left column).

We observed that synchrony in spontaneous activity (measured during fixation on a blank screen) is highly correlated with synchrony driven by our visual stimuli ($r > 0.86$ for both LFP frequency bands). This suggests that unknown factors, other than RF overlap and difference in preferred directions, are also important for determining synchrony strength. As shown in Table 2 (middle column), adding a factor to the GLM to account for synchrony in spontaneous activity explained a substantial additional portion of the variance (9%–56%). For synchrony in the gamma band LFP, adding spontaneous synchrony to the model increased the r^2 value from 0.521 to 0.881.

In sharp contrast, adding feature grouping (one versus two objects) to the GLM model only accounts for an additional 0.1% of the variance in synchrony strength for the gamma band LFP. Similarly weak effects of adding feature grouping to the GLM model are seen for the other synchrony metrics, as shown in Table 2 (right column). Even if only data from the one bar versus two bar experiment are analyzed, the maximum additional variance accounted for by feature grouping is 2.5% (gamma band MU activity). These results show that synchrony is much more tightly linked to RF parameters than to feature grouping.

Discriminability of Feature Grouping Using Synchrony

When synchrony strength depended on the stimulus configuration, the effects were typically quite small relative to the variability across pairs of recording sites (e.g., Figure 2A). This raises the question of how reliably one could discriminate between stimulus conditions (e.g., one figure versus two) based on measurements of synchrony. We reasoned that, if neuronal circuits are able to compensate somehow for local variations in synchrony strength, then the differential synchrony seen in Figures 2–6 might become a more robust signal for detecting grouped features.

To test this possibility, we applied ROC analysis to the residuals of the GLM described above that employed spontaneous synchrony, RF overlap, difference in preferred directions, and monkey identity as the independent variables. The residuals of the model were sorted into two groups (one object versus two objects) and analyzed by an ideal observer implemented using ROC analysis. The ideal observer was charged with the task of determining whether one object or two objects was presented based on the distribution of synchrony metrics across the population of recording sites. This is equivalent to randomly choosing a pair of recording sites driven by one object and a pair of sites driven by two objects, and quantifying how often synchrony was stronger for the pair of sites responding to the single

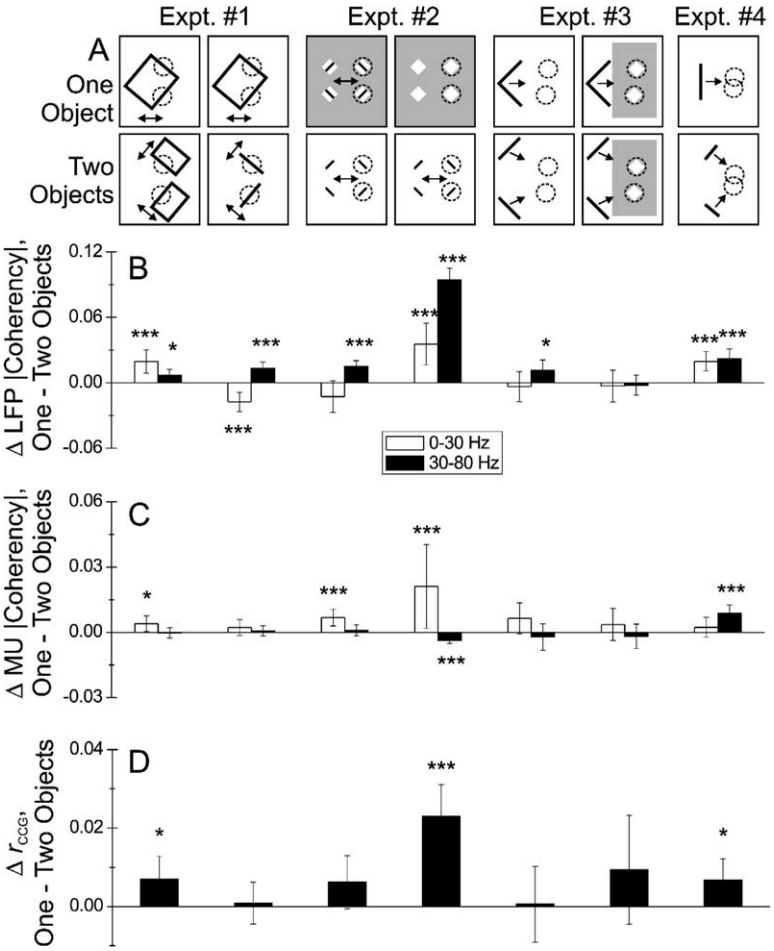

Figure 6. Summary of Results for All Four Experiments

(A) The seven stimulus conditions studied are shown above the columns of data. Top row: stimulus conditions containing a single ("bound") object. Bottom row: stimulus conditions containing two separate ("unbound") objects.

(B) Summary of LFP coherency data. The mean (±2 SE) difference in coherency magnitude between one object and two objects is plotted for each stimulus condition. Open and filled bars indicate data from the 0–30 Hz and 30–80 Hz bands, respectively. The BBS hypothesis predicts that all values should be significantly larger than zero. Significance is indicated as follows: *$p < 0.05$; **$p < 0.01$; ***$p < 0.001$.

(C) Summary of MU coherency data.

(D) Summary of MU synchrony based on the r_{CCG} metric.

figure (see Discussion). Importantly, this model assumes that variations in synchrony strength with the parameters described above are somehow compensated by the cortical circuitry. This may not be a realistic assumption, but this model provides a reasonable upper limit for the reliability of synchrony as a code for feature grouping.

Figure 7 shows the results of this ideal observer analysis for both LFP and MU signals. The BBS hypothesis predicts that the performance of the ideal observer should be significantly larger than 50% correct in all stimulus conditions. Indeed, performance was significantly better than chance for experiment 4 (one bar versus two bars), and this was true for LFP |Coherency| (Figure 7B), MU |Coherency| (Figure 7C), and MU r_{CCG} metrics (Figure 7D). Ideal observer performance was also significantly better than chance for the one figure versus two figures condition of experiment 1 (first column of Figure 7), but this effect was not maintained for the one figure versus two bars condition (second column of Figure 7). Ideal observer performance was highly reliable only for the mask only condition of experiment 2, in which no moving features were presented. In experiment 3, in which stimulus differences around the RFs were smallest, discrimination performance was not significantly better than chance. Moreover, even for experiment 4, performance of the ideal observer did not exceed 61% correct, despite the fact that our analysis compensated for local variations in synchrony strength due to RF overlap, difference in preferred directions, etc. This suggests that, even in the most optimistic setting, synchrony between pairs of recording sites does not provide a very reliable code for feature grouping.

Discussion

Although the BBS hypothesis has been questioned on theoretical and practical grounds (Ghose and Maunsell, 1999; Shadlen and Movshon, 1999), it is nevertheless critical to establish empirically whether or not synchrony is a reliable neural correlate of feature grouping. Our studies have extended previous tests of the BBS hypothesis in three important ways. (1) Whereas most previous studies have compared stimulus conditions that differed within the classical RFs (Castelo-Branco et al., 2000; Engel et al., 1991a; Engel et al., 1991b; Gail et al., 2000; Kreiter and Singer, 1996; Lamme and Spekreijse, 1998; Livingstone, 1996; Thiele and Stoner, 2003), we have tailored our stimuli (experiments 1–3) to be identical within the classical RFs of the recorded neurons. In addition, using partially occluded displays

Table 1. Dependence of Synchrony Strength on RF Overlap and Difference in Preferred Directions

	RF Overlap		Difference in Preferred Directions	
0–30 Hz LFP	$p < 10^{-15}$	r = 0.29	$p < 10^{-4}$	r = −0.15
30–80 Hz LFP	$p < 10^{-15}$	r = 0.63	p = 0.04	r = −0.07
0–30 Hz MU	$p < 10^{-9}$	r = 0.21	$p < 10^{-5}$	r = −0.15
30–80 Hz MU	$p < 10^{-15}$	r = 0.31	$p < 10^{-7}$	r = −0.19
r_{CCG}	$p < 10^{-12}$	r = 0.24	$p < 10^{-7}$	r = −0.19

(experiment 3), we have compared synchrony in response to bound versus unbound features while limiting stimulus differences to regions well outside of the RF boundaries. Although synchrony does depend on stimulus differences immediately around the classical RFs, as reported previously (Bretzner et al., 2000; Bretzner et al., 2001), we find that synchrony is not consistently related to feature grouping per se. When stimulus differences are confined to regions further away from the classical RF using partial occlusion (experiment 3), the dependence of synchrony on grouping is diminished. (2) Unlike previous studies, we have focused most of our experiments on pairs of recording sites with RFs that are nonoverlapping *and* noncollinear. This provides a more general test of the BBS hypothesis, as described in the Introduction. Whereas previous studies have reported that synchrony depends on feature grouping for groups of neurons with nonoverlapping, collinear RFs (Brosch et al., 1997; Freiwald et al., 1995; Gray et al., 1989), our findings show that this result does not generalize to noncollinear RFs. When we also examine pairs of recording sites with overlapping RFs, we find that synchrony strength depends much more strongly on RF overlap and difference in preferred directions than on feature grouping. Unknown factors must also contribute strongly to synchrony among our recording sites, since the addition of spontaneous synchrony to our statistical model accounts for a substantial portion of the variance in the data. In contrast, incorporating feature grouping into our model accounted for at most an additional 2.5% of variance, and more typically less than 1% (Table 2). Thus, at least in MT, the BBS hypothesis does not apply to the vast majority of pairs of visual RFs, which are both nonoverlapping and noncollinear. (3) We have assessed the reliability of synchrony as a code for feature grouping by employing ideal observer models that operate on the measured distributions of synchrony strength across our sample of recording sites. Even when we assume that local variations in synchrony strength are fully compensated by the cortical circuitry (which seems unlikely), the performance of our ideal observer is poor. This result lies in stark contrast to previous single-unit studies in MT, in which an ideal observer of single-unit firing rates across trials could discriminate among visual stimuli with fidelity comparable to that of the animal (Britten et al., 1992; Uka and DeAngelis, 2003). Together, our observations suggest that synchrony in area MT does not provide a robust neural code for feature grouping.

Although we have attempted to maximize detection of feature grouping from our population measurements of synchrony, it must be acknowledged that we do not know how neural circuits in the brain might actually decode synchrony. It is possible, for example, that only groups of neurons exhibiting the strongest synchrony contribute to perceptual binding. In this case, we might underestimate the usefulness of synchrony as a code for feature grouping. It is also possible that our linear statistical model (GLM) does not capture all of the information conveyed by synchrony about binding. While we cannot rule out these possibilities, we note that it will be critical for proponents of the BBS hypothesis to demonstrate that synchrony can reliably predict behavior.

We have chosen stimulus configurations in which simple moving features were grouped or not depending on stimulus context outside of the classical RFs. Although the differences between our bound and unbound conditions are readily apparent to most observers (see stimulus examples at http://cabernet.wustl.edu/~gregd/binding_animations), we do not know the perceptual status of our monkey observers, since the animals were simply required to fixate in these experiments. Thus, it is possible that our monkeys did not experience the intended grouping percepts in some of our stimuli (e.g., experiment 3). We think that this is unlikely to explain our overall pattern of results, however, and we note that the same limitation applies to the vast majority of previous studies on the role of synchrony in feature grouping (e.g., Brosch et al., 1997; Castelo-Branco et al., 2000; Engel et al., 1991a; Gail et al., 2000; Gray et al., 1989; Kreiter and Singer, 1996).

Table 2. Variance Accounted for by Different Versions of a GLM

	GLM, Difference in Preferred Directions, RF Overlap, Monkey: r^2	Addition of Spontaneous Synchrony: r^2	Addition of Feature Grouping: r^2
0–30 Hz LFP	0.259	0.820	0.820
30–80 Hz LFP	0.521	0.881	0.882
0–30 Hz MU	0.064	0.157	0.163
30–80 Hz MU	0.132	0.164	0.166
r_{CCG}	0.097	0.151	0.157

Left column: base model includes RF overlap, difference in preferred directions, and monkey identity. Middle column: base model plus a term to account for spontaneous synchrony. Right column: base model with terms for both spontaneous synchrony and feature grouping.

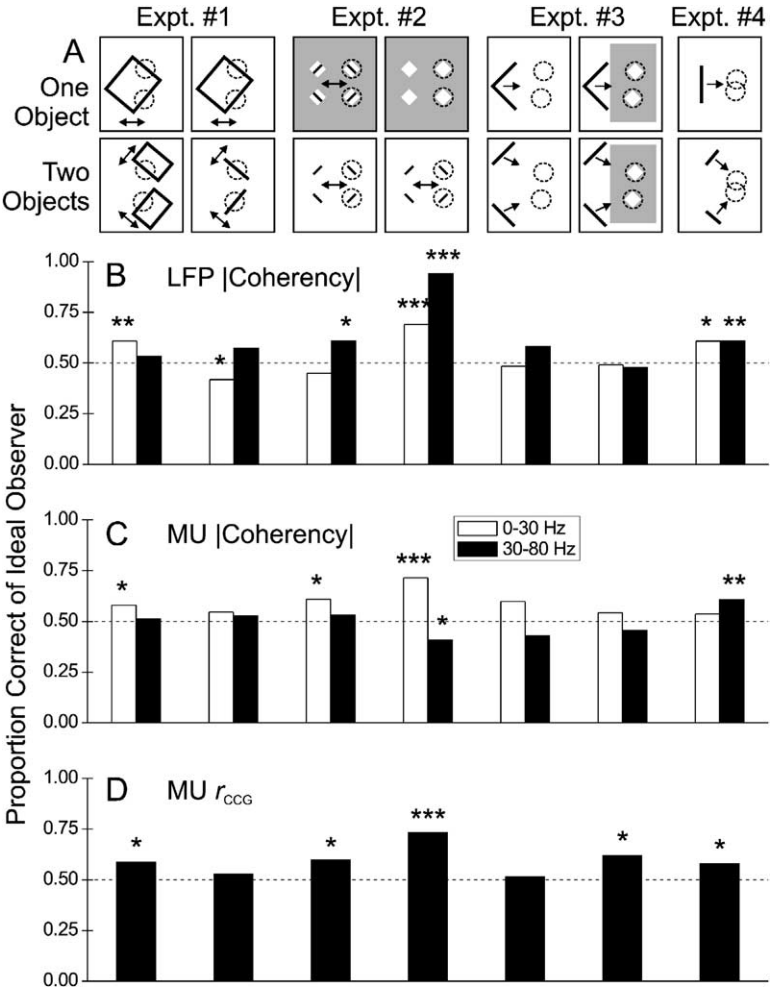

Figure 7. Summary of Ideal Observer Analysis for All Experiments

(A) Iconized depictions of the different stimulus conditions, as in Figure 6A.

(B) Ideal observer performance based on LFP coherency data is shown for each stimulus condition. Open and filled bars indicate data from the 0–30 Hz and 30–80 Hz bands, respectively. The dashed horizontal line indicates chance performance of the ideal observer. ROC values significantly different from 0.5 are indicated as follows: *$p < 0.05$; **$p < 0.01$; ***$p < 0.001$.

(C) Ideal observer performance based on MU coherency data.

(D) Ideal observer performance based on MU r_{CCG} data.

It is worth emphasizing that our application of ROC analysis in Figure 7 is quite different from that used previously in single-unit studies (e.g., Britten et al., 1992; Uka and DeAngelis, 2003). Whereas those studies operated on distributions of single-trial firing rates from single neurons, our application of ROC analysis here operates on distributions of trial-averaged synchrony metrics across many pairs of recording sites. Estimates of synchrony strength on individual trials are very noisy, such that an ideal observer cannot discriminate between one figure versus two figures based on single-trial estimates of synchrony from a pair of recording sites (data not shown). Thus, we adopted the present analysis as a best case scenario. Note that the synchrony metric for each pair of recording sites is the average across many stimulus repetitions; hence, our analysis essentially allows for some pooling of neuronal responses (assuming ergodicity). Although this best case scenario is not a standard neural application of ROC analysis, the fact that the ideal observer performance is poor only underscores the unreliability of MT synchrony as a code for feature binding, relative to the ability of single MT neurons to signal direction or depth (Britten et al., 1992; Uka and DeAngelis, 2003).

A potential criticism of this study is that our analysis methods may not have been sufficiently sensitive to detect changes in neuronal synchrony with feature grouping. To address this issue, we performed extensive numerical simulations (data not shown). We generated independent spike trains with PSTHs matched to those of a typical data set (Oram et al., 1999), and we then added various known percentages of correlated spikes to these independent trains. Using each of our synchrony metrics, we quantified the ability of our ideal observer model to discriminate between spike trains with no correlated spikes and spike trains with a known percentage of correlated spikes. We matched the firing rates and numbers of trials in our simulations to a typical MU data set. Our simulations revealed that the |Coherency|, and r_{CCG} metrics could reliably detect (at a 75% correct criterion) the addition of approximately 2% correlated spikes. By comparison, the NC metric (Konig, 1994; Kreiter and Singer, 1996) was approximately 3- to 4-fold less sensitive. Based on these simulations, our failure to observe significant synchrony in many of our MU recordings suggests that any changes in the percentage of synchronous spikes must have been on the order of 1% or less.

After finding very little synchrony among pairs of MU recordings with nonoverlapping RFs, we attempted to

replicate the results of Kreiter and Singer (1996). In these experiments, the RFs were overlapping, and the stimuli (one intermediate bar versus two optimal bars) differed within the classical RFs. We replicated the finding that synchrony is stronger for the single bar stimulus, but the effect in our data set (Figure 5) was much smaller than that reported by Kreiter and Singer. Sampling bias appears to be a likely explanation for this discrepancy. Kreiter and Singer (1996) did not collect data from pairs of MT sites "if, after sampling of a few sweeps, no correlation was observed" (p. 2382), and they do not state the percentage of sites that were discarded by this criterion. In contrast, we recorded from all pairs of sites to which we could tailor our stimuli, with no criteria based on synchrony strength. If, for example, we were to exclude all pairs of our recording sites with NC < 25% (Figure 5D), then our results would more closely resemble those of Kreiter and Singer, although we would still have some pairs of recording sites with stronger synchrony for two bars than one bar.

In conclusion, our results from area MT suggest that the BBS hypothesis, in its strongest form (Singer, 1997), does not hold. For nonoverlapping, noncollinear RFs, synchrony is not a reliable predictor of feature grouping. Among neurons with overlapping or collinear RFs, synchrony may contribute to perceptual feature grouping or may simply be a reflection of local cortical connectivity (Lamme and Spekreijse, 1998). Disentangling these two possibilities requires experiments that directly correlate synchrony with perceptual feature binding in a controlled psychophysical task. This has recently been attempted in V2 by Woelbern et al. (2002), but it is not possible to distinguish between effects of attention and effects of feature grouping in their study (as the authors acknowledge). A recent study (Roelfsema et al., 2004) has found that synchrony among V1 neurons with nonoverlapping RFs does not correlate with perceptual performance in a curve-tracing task, consistent with our conclusions regarding MT. Thus, the available evidence suggests that we either reject the BBS hypothesis or conclude that synchrony has a limited role in feature grouping that is restricted to overlapping and/or collinear RFs.

Although our findings cast doubt on the role of synchrony in spatial grouping of visual features, synchrony may still play other important roles in the mammalian brain. For example, synchrony has been proposed as a mechanism for selective attention (Fries et al., 2001; Steinmetz et al., 2000), memory processing (Harris et al., 2003; Kirk and Mackay, 2003; Seidenbecher et al., 2003), and sensorimotor integration (Bland and Oddie, 2001; Riehle et al., 1997; Roelfsema et al., 1997). Further work will be necessary to demonstrate a causal role for synchrony in these brain functions.

Experimental Procedures

Preparation

Scleral search coils, a head restraint post, and an MT recording chamber were implanted in each of two male rhesus monkeys (*Macaca mulatta*) as described previously (DeAngelis and Uka, 2003). Monkeys were trained through operant conditioning to maintain fixation within a 1.2°–1.6° window (full width) in order to receive liquid rewards. Typically, recording sessions lasted 3–5 hr, during which the monkey completed 1000–2000 trials. During each session, a multielectrode positioning system (Alpha Omega Engineering) was used to insert a pair of tungsten microelectrodes (impedance 0.5–1 MΩ; FHC, Inc.) into the cortex through transdural guide tubes. The guide tubes were separated by a distance of 1–5 mm within a grid of holes (1 mm spacing) located inside the recording chamber (Crist Instruments). However, because the gray matter of area MT is oriented obliquely relative to the guide tubes (DeAngelis and Newsome, 1999), the tip separation of the electrodes could be substantially larger than the separation of the guide tubes and was not precisely known. Thus, we gauged the distance between electrode tips by the separation of the MT RFs, given that area MT has a clear retinotopic organization (Maunsell and Van Essen, 1987). Recording locations were assigned to area MT based on gray-to-white matter transitions, recording depth, direction and speed tuning of single units and MU clusters, the ratio of RF size to eccentricity, and the subsequent entry of electrodes into gray matter with properties typical of area MST.

Data Acquisition

Raw neural signals were amplified (AM systems) and then processed separately to derive LFP and MU recordings. LFP signals were obtained by filtering the raw neural signal from 1 to 200 Hz (8-pole filters) and then sampling at 500 Hz. These potentials are thought to represent the aggregate pre- and postsynaptic activity from clusters of neurons around the electrode tip (Mitzdorf, 1985). MU recordings were obtained by first filtering the raw neural signals from 250 Hz to 6 kHz, and then thresholding the signals using conventional voltage-time window discriminators (Bak Electronics) to generate MU events that were time stamped with 1 ms resolution. We set the window discriminator thresholds so that the spontaneous firing rates for MU activity ranged from 50 to 100 events/s. The peak firing rates of visually evoked responses generally ranged from 200 to 500 events/s.

Horizontal and vertical eye traces were sampled at 500 Hz and stored to disk at 250 Hz. Data acquisition was coordinated using TEMPO software (Reflective Computing).

Visual Stimulation

Visual stimuli were generated using an OpenGL accelerator board (3DLabs Oxygen GVX1) running at a refresh rate of 100 Hz. The positions of all moving stimuli (bars and polygons) were updated every video frame, and hardware anti-aliasing algorithms were used to achieve subpixel resolution and smooth motion. For accurate determination of the start of visual stimulation on each trial, a TTL pulse was outputted at the beginning of each video frame following the start of stimulus onset, and these pulses were time stamped with 1 ms resolution. Visual stimuli were displayed on a 21 inch CRT (Iiyama) that subtended 40° × 30° of visual angle at the viewing distance of 57 cm.

Experimental Protocol

An interactive RF mapping program was first used to qualitatively characterize the direction and speed tuning, RF location, and RF size of MU responses from each of the two microelectrodes in MT. Next, we quantitatively measured the direction tuning curve for each recording site by presenting moving bars at eight directions of motion, 45° apart. The bar stimuli were oriented perpendicular to their direction of movement and moved at the preferred speed of the neurons. After each sweep through the RF, the bar reappeared on the opposite edge of the RF and swept through again until the 1.5 s stimulus duration expired. MU responses were fit with a Gaussian, and the preferred direction of motion for each recording site was determined from the peak of the Gaussian fit.

Following the direction tuning measurement, quantitative RF mapping was carried out by presenting drifting sine wave grating patches (1–2 cycles/degree, 5–10 cycles/s) at all locations on a 4 × 4 grid that was centered over the RF and was roughly twice the RF diameter. Typically, the width of each square grating patch was one-quarter of the estimated RF diameter. MU responses were fit online with a two-dimensional Gaussian to obtain quantitative estimates of RF center location and size (±1 SD of the Gaussian fit). The results of these fits were used to calculate a quantitative index

of the overlap of the two RFs, defined as the area of the intersection of the two Gaussians divided by the area of the smaller RF.

After RF mapping, we tailored the stimuli to the RFs (see Figure 1A) based on the direction and speed preferences of the two recording sites, as well as the locations and overlap of the RFs. This was done using an interactive program that superimposed the visual stimuli over the quantitative estimates of the two RFs and allowed the user to adjust the size, orientation, skewness, position, and motion of each stimulus figure. This enabled us to closely match the orientation/direction of one side of the moving figure to the direction preference of each neuron. If we could not match stimulus edge motion to the MT direction preference within 15°, we moved one electrode to find a more favorable pairing. We selected among pairs of MU recording sites that were direction selective with peak firing rates at least 2-fold larger than the level of spontaneous activity. The combination of RF locations and direction preferences made certain combinations of sites incompatible with our experiments. Specifically, pairs of recording sites with opposite direction preferences were not suitable, and pairs in which the preferred direction of one site pointed directly at the RF of the other site were also problematic. Importantly, however, recording sites were never selected based on the strength of synchrony between the constituent neurons.

When designing the stimuli, we tried to maximize the MU responses of the two recording sites while minimizing stimulus differences within the classical RFs. Thus, we tried to keep the corners of our figures outside of the classical RF. Similarly, in cases where the two RFs were stimulated by different objects, all attempts were made to activate each site by the edges of only one of the objects. In cases where objects were occluded by a mask, the mask appeared with the fixation point, 300 ms before the onset of the moving objects. Stimuli were presented for 3 s each (block randomized), and data were usually collected across 30 repetitions of each unique stimulus condition.

Data Analysis

We quantified synchrony in MU activity and LFPs using two general methods: spectral coherency analysis and conventional cross-correlation. We first describe the coherency analysis, which allows one to quantify the strength of signal correlations within specific frequency bands of interest (e.g., the gamma band). The coherency spectrum between two signals, *x* and *y*, is defined as

$$Coherency_{x,y}(f) = \frac{Sxy(f)}{\sqrt{Sxx(f) \times Syy(f)}}$$

where $Sxy(f)$ denotes the cross-spectrum, and $Sxx(f)$, $Syy(f)$ denote the auto-spectra of each signal. Note that the coherency is a complex quantity. We used multitaper spectral estimation (Thompson, 1982) to compute the auto- and cross-spectra of our MU spike trains and LFP signals. This methodology reduces the variance of spectral estimates by averaging independent estimates obtained with a set of orthogonal tapers (Mitra and Pesaran, 1999). Similar to Pesaran et al. (2002), we used nine Slepian prolate functions as data tapers. A |Coherency| spectrogram (see Figure 1E) was generated by computing coherency within overlapping 512 ms data segments that were successively offset by 100 ms intervals. Using these parameters, the frequency resolution of the |Coherency| spectrogram is approximately 10 Hz. To remove stimulus-locked covariations in activity from the |Coherency| spectrogram, we first computed PSTHs of MU and LFP responses by averaging these signals across repetitions of each distinct stimulus. We then subtracted the averaged PSTH from the MU and LFP responses in each trial. To verify that this method was effective at removing stimulus-coordinated activity from the |Coherency| spectrogram, we also generated "shuffled" |Coherency| spectrograms by shuffling the trial pairings of the signals from the two electrodes. These shuffled |Coherency| plots never showed any clear structure, confirming that stimulus-locked response covariations were eliminated.

To distill the |Coherency| spectrogram down into metrics that summarize synchrony strength, we performed the following steps. First, we defined two frequency bands of interest: 0–30 Hz, which encompasses the traditional frequency bands of the EEG, and 30–80 Hz, which is commonly referred to as the gamma band. Second, we defined periods of time in which responses on both electrodes were significantly larger than spontaneous activity. For this purpose, the MU spike trains were binned into 40 ms segments, and a Wilcoxon signed rank test was used to determine if the activity in each 40 ms bin was significantly greater than spontaneous activity ($p < 0.05$). We then identified continuous intervals of at least 100 ms in which the visual response from both electrodes was consistently larger than spontaneous activity. These periods often lasted several hundred milliseconds and were broken up into 100 ms chunks for some analyses (see below). Having defined the time and frequency windows of interest, we then averaged the complex coherency values across time, stimulus repetitions, and frequency within each frequency band of interest. The magnitude and phase of the resultant averaged coherency vector were then computed. We used the magnitude of the average coherency, |Coherency|, as our metric of synchrony strength, which is bounded between 0 (no correlation) and 1 (perfect correlation). The phase of the averaged coherency was generally very close to zero and was not used further in the analysis.

In addition to spectral coherency, we also analyzed synchrony using conventional cross-correlation analysis (Bair et al., 2001). For each 100 ms time segment in which responses were significantly larger than spontaneous activity, we compiled cross-correlograms by averaging across repetitions of each unique stimulus. Correlograms were corrected for finite sample length by normalizing with a triangle function (Bair et al., 2001). We also computed a shuffled correlogram by pairing the spike train from one recording site with each of the spike trains (across trial repetitions) from the other recording site. This shuffled correlogram will reflect stimulus-driven coordination of the two responses but should destroy correlations of neural origin (Perkel et al., 1967). We subtracted the shuffled correlogram from each raw correlogram. As our primary measure of cross-correlation strength, we computed the r_{CCG} metric (Bair et al., 2001), also known as the NCC metric (Thiele and Stoner, 2003). The r_{CCG} was calculated as follows:

$$r_{CCG} = \frac{CCG}{\sqrt{ACG1 \times ACG2}}$$

where the areas under the shuffle-subtracted cross-correlogram (CCG) and auto-correlograms (ACG1 and ACG2) were calculated over time lags between –5 ms and +5 ms.

To directly compare our measures of synchrony with those of Kreiter and Singer (1996), we also calculated their NC metric, which is based on fitting Gabor functions to the raw cross-correlograms (Konig, 1994). NC measures the frequency of synchronized spikes relative to the frequency of spuriously aligned spikes and is computed as the amplitude of the raw correlogram peak normalized by the correlogram baseline.

Supplemental Data

The Supplemental Data include two supplemental figures and can be found with this article online at http://www.neuron.org/cgi/content/full/46/2/333/DC1/.

Acknowledgments

We thank Amy Wickholm and Heidi Loschen for excellent technical support and monkey training. We are grateful to Dora Angelaki, Tim Holy, Larry Snyder, Jacob Nadler, Ben Kolber, Jerry Nguyenkim, Yong Gu, Chris Fetsch, Vinod Rao, and Dan Christiansen for helpful comments on the manuscript. This work was supported by the National Eye Institute (EY-013644), and by a Burroughs-Wellcome Career Award in the Biomedical Sciences (to G.C.D.). B.J.A.P. was supported by a Vision Sciences Training Grant from the NEI.

Received: August 11, 2004
Revised: January 10, 2005
Accepted: March 1, 2005
Published: April 20, 2005

References

Allman, J., Miezin, F., and McGuinness, E. (1985). Direction- and velocity-specific responses from beyond the classical receptive

field in the middle temporal visual area (MT). Perception *14*, 105–126.

Bair, W., Zohary, E., and Newsome, W.T. (2001). Correlated firing in macaque visual area MT: time scales and relationship to behavior. J. Neurosci. *21*, 1676–1697.

Bedenbaugh, P., and Gerstein, G.L. (1997). Multiunit normalized cross correlation differs from the average single-unit normalized correlation. Neural Comput. *9*, 1265–1275.

Bland, B.H., and Oddie, S.D. (2001). Theta band oscillation and synchrony in the hippocampal formation and associated structures: the case for its role in sensorimotor integration. Behav. Brain Res. *127*, 119–136.

Bretzner, F., Aitoubah, J., Shumikhina, S., Tan, Y.F., and Molotchnikoff, S. (2000). Stimuli outside the classical receptive field modulate the synchronization of action potentials between cells in visual cortex of cats. Neuroreport *11*, 1313–1317.

Bretzner, F., Aitoubah, J., Shumikhina, S., Tan, Y.F., and Molotchnikoff, S. (2001). Modulation of the synchronization between cells in visual cortex by contextual targets. Eur. J. Neurosci. *14*, 1539–1554.

Britten, K.H., Shadlen, M.N., Newsome, W.T., and Movshon, J.A. (1992). The analysis of visual motion: a comparison of neuronal and psychophysical performance. J. Neurosci. *12*, 4745–4765.

Brosch, M., Bauer, R., and Eckhorn, R. (1997). Stimulus-dependent modulations of correlated high-frequency oscillations in cat visual cortex. Cereb. Cortex *7*, 70–76.

Castelo-Branco, M., Goebel, R., Neuenschwander, S., and Singer, W. (2000). Neural synchrony correlates with surface segregation rules. Nature *405*, 685–689.

DeAngelis, G.C., and Newsome, W.T. (1999). Organization of disparity-selective neurons in macaque area MT. J. Neurosci. *19*, 1398–1415.

DeAngelis, G.C., and Uka, T. (2003). Coding of horizontal disparity and velocity by MT neurons in the alert Macaque. J. Neurophysiol. *89*, 1094–1111.

Eckhorn, R., Bauer, R., Jordan, W., Brosch, M., Kruse, W., Munk, M., and Reitboeck, H.J. (1988). Coherent oscillations: a mechanism of feature linking in the visual cortex? Multiple electrode and correlation analyses in the cat. Biol. Cybern. *60*, 121–130.

Engel, A.K., Konig, P., Gray, C.M., and Singer, W. (1990). Stimulus-dependent neuronal oscillations in cat visual cortex: Inter-columnar interaction as determined by cross-correlation analysis. Eur. J. Neurosci. *2*, 588–606.

Engel, A.K., Konig, P., and Singer, W. (1991a). Direct physiological evidence for scene segmentation by temporal coding. Proc. Natl. Acad. Sci. USA *88*, 9136–9140.

Engel, A.K., Kreiter, A.K., Konig, P., and Singer, W. (1991b). Synchronization of oscillatory neuronal responses between striate and extrastriate visual cortical areas of the cat. Proc. Natl. Acad. Sci. USA *88*, 6048–6052.

Freiwald, W.A., Kreiter, A.K., and Singer, W. (1995). Stimulus dependent intercolumnar synchronization of single unit responses in cat area 17. Neuroreport *6*, 2348–2352.

Frien, A., and Eckhorn, R. (2000). Functional coupling shows stronger stimulus dependency for fast oscillations than for low-frequency components in striate cortex of awake monkey. Eur. J. Neurosci. *12*, 1466–1478.

Frien, A., Eckhorn, R., Bauer, R., Woelbern, T., and Kehr, H. (1994). Stimulus-specific fast oscillations at zero phase between visual areas V1 and V2 of awake monkey. Neuroreport *5*, 2273–2277.

Fries, P., Roelfsema, P.R., Engel, A.K., Konig, P., and Singer, W. (1997). Synchronization of oscillatory responses in visual cortex correlates with perception in interocular rivalry. Proc. Natl. Acad. Sci. USA *94*, 12699–12704.

Fries, P., Reynolds, J.H., Rorie, A.E., and Desimone, R. (2001). Modulation of oscillatory neuronal synchronization by selective visual attention. Science *291*, 1560–1563.

Gail, A., Brinksmeyer, H.J., and Eckhorn, R. (2000). Contour decouples gamma activity across texture representation in monkey striate cortex. Cereb. Cortex *10*, 840–850.

Ghose, G.M., and Maunsell, J. (1999). Specialized representations in visual cortex: a role for binding? Neuron *24*, 79–85, 111–125.

Gilbert, C.D., and Wiesel, T.N. (1979). Morphology and intracortical projections of functionally characterised neurones in the cat visual cortex. Nature *280*, 120–125.

Gilbert, C.D., and Wiesel, T.N. (1983). Clustered intrinsic connections in cat visual cortex. J. Neurosci. *3*, 1116–1133.

Gilbert, C.D., and Wiesel, T.N. (1989). Columnar specificity of intrinsic horizontal and corticocortical connections in cat visual cortex. J. Neurosci. *9*, 2432–2442.

Golledge, H.D., Hilgetag, C.C., and Tovee, M.J. (1996). A solution to the binding problem? Information processing. Curr. Biol. *6*, 1092–1095.

Golledge, H.D., Panzeri, S., Zheng, F., Pola, G., Scannell, J.W., Giannikopoulos, D.V., Mason, R.J., Tovee, M.J., and Young, M.P. (2003). Correlations, feature-binding and population coding in primary visual cortex. Neuroreport *14*, 1045–1050.

Gray, C.M. (1999). The temporal correlation hypothesis of visual feature integration: still alive and well. Neuron *24*, 31–47, 111–125.

Gray, C.M., Konig, P., Engel, A.K., and Singer, W. (1989). Oscillatory responses in cat visual cortex exhibit inter-columnar synchronization which reflects global stimulus properties. Nature *338*, 334–337.

Halliday, D.M., and Rosenberg, J.R. (1999). Modern Techniques in Neuroscience Research. In Modern Techniques in Neuroscience Research, U. Windhorst and H. Johansson, eds. (Berlin: Springer-Verlag), pp. 503–543.

Harris, K.D., Csicsvari, J., Hirase, H., Dragoi, G., and Buzsaki, G. (2003). Organization of cell assemblies in the hippocampus. Nature *424*, 552–556.

Kirk, I.J., and Mackay, J.C. (2003). The role of theta-range oscillations in synchronising and integrating activity in distributed mnemonic networks. Cortex *39*, 993–1008.

Kisvarday, Z.F., Beaulieu, C., and Eysel, U.T. (1993). Network of GABAergic large basket cells in cat visual cortex (area 18): implication for lateral disinhibition. J. Comp. Neurol. *327*, 398–415.

Kisvarday, Z.F., Toth, E., Rausch, M., and Eysel, U.T. (1997). Orientation-specific relationship between populations of excitatory and inhibitory lateral connections in the visual cortex of the cat. Cereb. Cortex *7*, 605–618.

Konig, P. (1994). A method for the quantification of synchrony and oscillatory properties of neuronal activity. J. Neurosci. Methods *54*, 31–37.

Kreiter, A.K., and Singer, W. (1996). Stimulus-dependent synchronization of neuronal responses in the visual cortex of the awake macaque monkey. J. Neurosci. *16*, 2381–2396.

Lamme, V.A., and Spekreijse, H. (1998). Neuronal synchrony does not represent texture segregation. Nature *396*, 362–366.

Livingstone, M.S. (1996). Oscillatory firing and interneuronal correlations in squirrel monkey striate cortex. J. Neurophysiol. *75*, 2467–2485.

Lorenceau, J., and Shiffrar, M. (1992). The influence of terminators on motion integration across space. Vision Res. *32*, 263–273.

Maunsell, J.H., and Van Essen, D.C. (1987). Topographic organization of the middle temporal visual area in the macaque monkey: representational biases and the relationship to callosal connections and myeloarchitectonic boundaries. J. Comp. Neurol. *266*, 535–555.

Mitra, P.P., and Pesaran, B. (1999). Analysis of dynamic brain imaging data. Biophys. J. *76*, 691–708.

Mitzdorf, U. (1985). Current source-density method and application in cat cerebral cortex: investigation of evoked potentials and EEG phenomena. Physiol. Rev. *65*, 37–100.

Oram, M.W., Wiener, M.C., Lestienne, R., and Richmond, B.J. (1999). Stochastic nature of precisely timed spike patterns in visual system neuronal responses. J. Neurophysiol. *81*, 3021–3033.

Perkel, D.H., Gerstein, G.L., and Moore, G.P. (1967). Neuronal spike trains and stochastic point processes. II. Simultaneous spike trains. Biophys. J. *7*, 419–440.

Pesaran, B., Pezaris, J.S., Sahani, M., Mitra, P.P., and Andersen,

R.A. (2002). Temporal structure in neuronal activity during working memory in macaque parietal cortex. Nat. Neurosci. *5*, 805–811.

Riehle, A., Grun, S., Diesmann, M., and Aertsen, A. (1997). Spike synchronization and rate modulation differentially involved in motor cortical function. Science *278*, 1950–1953.

Riesenhuber, M., and Poggio, T. (1999). Are cortical models really bound by the "binding problem"? Neuron *24*, 87–93, 111–125.

Rockland, K.S., and Lund, J.S. (1983). Intrinsic laminar lattice connections in primate visual cortex. J. Comp. Neurol. *216*, 303–318.

Roelfsema, P.R., Engel, A.K., Konig, P., and Singer, W. (1997). Visuomotor integration is associated with zero time-lag synchronization among cortical areas. Nature *385*, 157–161.

Roelfsema, P.R., Lamme, V.A., and Spekreijse, H. (2004). Synchrony and covariation of firing rates in the primary visual cortex during contour grouping. Nat. Neurosci. *7*, 982–991.

Seidenbecher, T., Laxmi, T.R., Stork, O., and Pape, H.C. (2003). Amygdalar and hippocampal theta rhythm synchronization during fear memory retrieval. Science *301*, 846–850.

Shadlen, M.N., and Movshon, J.A. (1999). Synchrony unbound: a critical evaluation of the temporal binding hypothesis. Neuron *24*, 67–77, 111–125.

Singer, W. (1997). Time as coding space in neocortical processing: a hypothesis. In The Cognitive Neurosciences, M.S. Gazzaniga, ed. (Cambridge, MA: MIT Press), pp. 91–104.

Singer, W. (1999). Neuronal synchrony: a versatile code for the definition of relations? Neuron *24*, 49–65, 111–125.

Singer, W., and Gray, C.M. (1995). Visual feature integration and the temporal correlation hypothesis. Annu. Rev. Neurosci. *18*, 555–586.

Steinmetz, P.N., Roy, A., Fitzgerald, P.J., Hsiao, S.S., Johnson, K.O., and Niebur, E. (2000). Attention modulates synchronized neuronal firing in primate somatosensory cortex. Nature *404*, 187–190.

Thiele, A., and Stoner, G. (2003). Neuronal synchrony does not correlate with motion coherence in cortical area MT. Nature *421*, 366–370.

Thompson, D.J. (1982). Spectrum estimation and harmonic analysis. Proc. IEEE *70*, 1055–1996.

Treisman, A. (1996). The binding problem. Curr. Opin. Neurobiol. *6*, 171–178.

Ts'o, D.Y., Gilbert, C.D., and Wiesel, T.N. (1986). Relationships between horizontal interactions and functional architecture in cat striate cortex as revealed by cross-correlation analysis. J. Neurosci. *6*, 1160–1170.

Uka, T., and DeAngelis, G.C. (2003). Contribution of middle temporal area to coarse depth discrimination: comparison of neuronal and psychophysical sensitivity. J. Neurosci. *23*, 3515–3530.

von der Malsburg, C. (1995). Binding in models of perception and brain function. Curr. Opin. Neurobiol. *5*, 520–526.

von der Malsburg, C., and Schneider, W. (1986). A neural cocktail-party processor. Biol. Cybern. *54*, 29–40.

Woelbern, T., Eckhorn, R., Frien, A., and Bauer, R. (2002). Perceptual grouping correlates with short synchronization in monkey prestriate cortex. Neuroreport *13*, 1881–1886.

Wolfe, J.M., and Cave, K.R. (1999). The psychophysical evidence for a binding problem in human vision. Neuron *24*, 11–17, 111–125.